JACS
JOURNAL OF THE AMERICAN CHEMICAL SOCIETY

Article

pubs.acs.org/JACS

Molecular Dynamics Simulations of Aldol Condensation Catalyzed by Alkylamine-Functionalized Crystalline Silica Surfaces

Ki Chul Kim,[†] Eric G. Moschetta,[‡] Christopher W. Jones,*[,‡] and Seung Soon Jang*[,†,§,∥]

[†]Computational NanoBio Technology Laboratory, School of Materials Science and Engineering, [‡]School of Chemical & Biomolecular Engineering, [§]Institute for Electronics and Nanotechnology, and [∥]Parker H. Petit Institute for Bioengineering and Bioscience, Georgia Institute of Technology, 771 Ferst Drive NW, Atlanta, Georgia 30332-0245, United States

Supporting Information

ABSTRACT: Molecular dynamics simulations are performed to investigate the cooperatively catalyzed aldol condensation between acetone and 4-nitrobenzaldehyde on alkylamine (or alkylenamine)-grafted silica surfaces, focusing on the mechanism of the catalytic activation of the acetone and 4-nitrobenzaldehyde by the acidic surface silanols followed by the nucleophilic attack of the basic amine functional group toward the activated reactant. From the analysis of the correlations between the catalytically active acid−base sites and reactants, it is concluded that the catalytic cooperativity of the acid−base pair can be affected by two factors: (1) the competition between the silanol and the amine (or enamine) to form a hydrogen bond with a reactant and (2) the flexibility of the alkylamine (or alkylenamine) backbone. Increasing the flexibility of the alkylamine facilitates the nucleophilic attack of the amine on the reactants. From the molecular dynamics simulations, it is found that C3 propylamine and C4 butylamine linkers exhibit the highest probability of reaction, which is consistent with the experimental observation that the activity of the aldol reaction on mesoporous silica depends on the length of alkylamine grafted on the silica surface. This simulation work serves as a pioneering study demonstrating how the molecular simulation approach can be successfully employed to investigate the cooperative catalytic activity of such bifunctional acid−base catalysts.

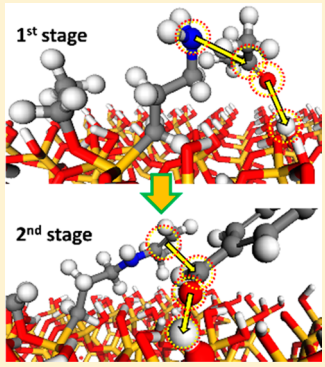

INTRODUCTION

Since the discovery of ordered mesoporous silicates, such as the M41S family of materials, with tailored pore sizes ranging from 2 to 10 nm and high surface areas around 1000 m^2/g,[1,2] mesoporous silica materials have attracted significant attention in the fields of catalysis,[3−14] gas separations,[15−19] and biorelated applications.[20,21] In particular, hybrid organic−inorganic mesoporous silica materials generated by incorporating organic basic functionalities on the surfaces have been explored as candidates for practical applications in catalysis and carbon capture.[3−8,22−29] For example, the combination of weakly acidic surface silanols coupled with basic amines functionalized on the mesoporous silica matrix is known to promote catalytic reactions such as the aldol condensation and nitroaldol condensation.[3−7,23,30−44] Regarding the bifunctional acid−base nature of these catalysts, Jones and co-workers have explored methodologies to enhance the catalytic rates by improving acid−base cooperativity in the model aldol condensation between acetone and 4-nitrobenzaldehyde.[3−8,22] They proposed a sequential two-stage cooperative catalytic reaction pathway for the aldol condensation: in the first stage, the acidic surface silanol protonates or forms a hydrogen bond with the acetone, and then the nucleophilic attack of the basic amine on the carbonyl carbon occurs, which generates an enamine; in the second stage, the C−C double bond of the enamine is used for the nucleophilic attack on the 4-nitrobenzaldehyde. Such a cooperative catalytic mechanism based on the acidic and basic functional groups could be evidenced by the reduced catalytic activity on either the bare mesoporous silica surfaces lacking the amines or the amine-functionalized mesoporous silica surfaces with inaccessible silanols deactivated by a hexamethyldisilazane-capping treatment.[7]

The catalytic cooperativity of the acid−base bifunctional mesoporous silica materials depends on their chemical (e.g., the relative acidity−basicity strength between the acid and base functional groups[5,6]) and physical (e.g., their proximity to each other, which can be affected by the relative ratio of acid to base,[23,30] the length and distribution of the alkylamines,[3,4] and pore sizes[4]) properties. A correlation between the acid strength and cooperative catalytic activity has been obtained using well-established ways for incorporating and controlling the surface acid strength of the mesoporous silica materials.[5,6,22,45] For example, Davis and co-workers demonstrated that weaker organic acids were better cooperative partners for primary amines than stronger acids.[35] Subsequent studies by Jones and co-workers reported that the modification of the silica surfaces by replacing weaker Brønsted acid silanols with stronger carboxylic acids had a negative impact on the catalytic activity for the aldol condensation between acetone and 4-nitrobenzaldehyde.[5,6] Likewise, considerable efforts have been

Received: March 31, 2016
Published: May 28, 2016

DOI: 10.1021/jacs.6b03309
J. Am. Chem. Soc. 2016, 138, 7664−7672

devoted to understanding the effect of the proximity between the acid and base functional groups on the cooperative catalytic activity for the aldol condensation. For example, Marin and co-workers examined the correlation of the relative ratio of the silanol to the amine on an alkylamine-functionalized mesoporous silica surface with the performance in the aldol condensation. They claimed that the best performance was obtained at a ratio of 1.7.[23] Jones and co-workers investigated cooperative acid−base interactions between silanols and aminoalkylsilanes on a mesoporous silica surface by changing the length of the alkylamine, ranging from an aminomethyl to an aminopentyl, for the aldol condensation.[3] They reported that the cooperative catalytic activity increased with the alkyl linker length up to an aminopropyl, whereas longer and more flexible alkyl linkers provided no further improvement of the cooperative catalytic activity. Subsequently, they verified that the optimal alkylamine length for maximum catalytic performance depended on the pore diameter of the mesoporous silica matrix.[4] It is inferred, therefore, that the proximity of each acid−base pair can be strongly impacted by the pore curvature as well as the length of the alkylamine.

Despite such efforts, many questions remain regarding the precise physical arrangement of the acids and bases on the silica surface and how this affects the cooperative catalytic activity. The acidic silanols are typically randomly distributed on the mesoporous silica surface, which leads to a difficulty in not only controlling the number of the silanols within access of the basic amines for cooperative catalysis but also sustaining a uniform spacing between the acid and base functional groups.[3−5,8,22,31] This ultimately results in a somewhat ambiguous understanding of the effect of each physical property (e.g., the length of the basic alkylamine and the distribution of the base functional groups on the surface) on the cooperative catalytic activity of the acid−base pairs. This challenge must be overcome for the rational design of an optimal mesoporous silica surface with suitable alkylamine functional groups. In this work, a molecular dynamics (MD) simulation approach is employed to quantitatively explore the role of the amine−silanol pairing in the cooperatively catalyzed model aldol condensation between acetone and 4-nitrobenzaldehyde. Using a silica surface model with a uniform distribution of silanol groups, specifically a crystalline α-quartz surface, the length of the alkylamine becomes the only variable to determine the proximity of each acid−base pair, and thereby the correlation between the length of the alkylamine and the cooperative catalytic activity can be clearly understood. Further investigation on the same surface with two alkylamine groups at three different alkylamine−alkylamine distances is performed to understand the effect of the distance between alkylamines on the cooperative catalytic activity. Through these investigations, we have systematically investigated the relationship between the cooperative catalytic activity and the dynamic motions of the reactant molecules and basic functional groups.

COMPUTATIONAL METHODS

All of the model structures simulated in this study were constructed using the simulation software Materials Studio (Accelrys Software Inc., San Diego, CA, USA). A crystalline silica (001) surface with the dimension of 5 nm × 5 nm × 10 nm was prepared from the bulk phase of the α-quartz. The silanol-terminated silica (001) surface consists of repeated siloxane bonds (Figure 1) as a slab structure with a thickness of 3 nm. Based on a proposed two-stage mechanism of the aldol condensation,[23,31,32,46] either an aminoalkyltriethoxysilane or ethoxyalkylenamine functional group was then grafted on the surface. The

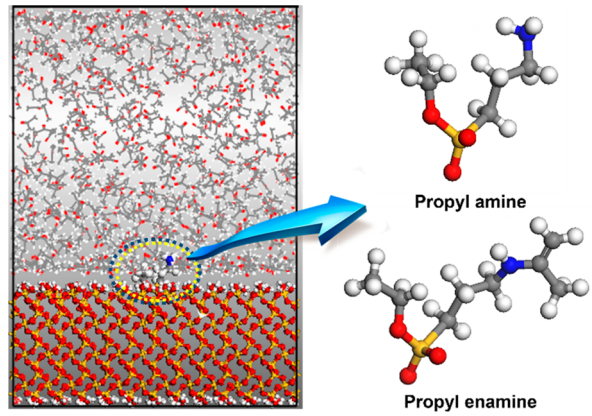

Figure 1. Simulated model structure of propylamine-functionalized crystalline silica surface surrounded by acetone molecules. The alkylenamine ($NH{-}CCH_2CH_3$) functional group is a reaction intermediate generated from the alkylamine (NH_2) once it reacts with a molecule of acetone. Hereafter, yellow, red, gray, white, and blue depict silicon, oxygen, carbon, hydrogen, and nitrogen, respectively.

aminoalkyltriethoxysilane has been reported to be postsynthetically grafted on the surface, leaving a bipodal structure by the reaction between one aminoalkyltriethoxysilane and two vicinal silanols.[47,48] Note that the enaminoalkyltriethoxysilane is an intermediate fragment generated by the catalytic reaction between the aminoalkyltriethoxysilane and acetone in the first stage of the proposed mechanism.[23,31,32,46] The length of the functional group was varied from C1 (methyl) to C4 (butyl). Figure 1 shows the chemical structures of the C3(propyl)-based amine and enamine functional groups. To consider the effect of the alkylamine−alkylamine distance as well as the length of the alkylamine, the systems with two alkylamines were also prepared to have alkylamine−alkylamine distances of either 8, 16, or 24 Å. Examples of crystalline silica surfaces with two aminopropyl or propylenamine functional groups at the alkylamine−alkylamine spacing of 8 Å are illustrated in Figure 2.

As described elsewhere[23,31,32,46] and stated earlier, the aldol condensation between acetone and 4-nitrobenzaldehyde is postulated to take place via the two-stage mechanism. In the first stage, the silanol

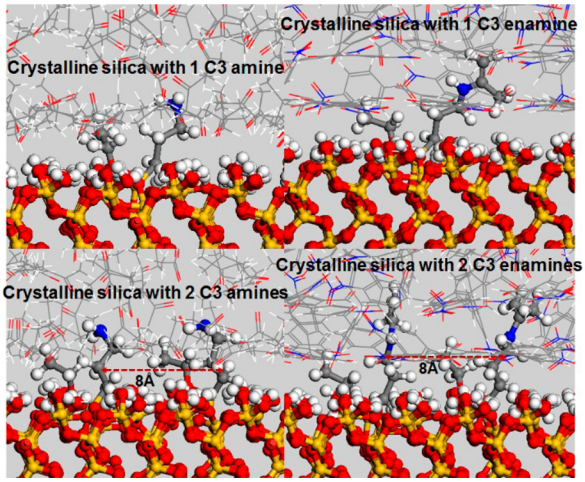

Figure 2. Snapshots of crystalline silica surfaces with either one or two functional groups, namely, C3(propyl)-amine or C3(propyl)-enamine, interacting with reactants. Two functional groups on the surfaces are separated at a distance of 8 Å. The top views of the models with two propylamines separated at distances of 8, 16, and 24 Å are shown in the Supporting Information.

DOI: 10.1021/jacs.6b03309
J. Am. Chem. Soc. 2016, 138, 7664−7672

and alkylamine cooperatively catalyze a neighboring acetone molecule to form an enamine fragment at the end of the alkylamine backbone. Subsequently, the enamine activates a neighboring 4-nitrobenzaldehyde that is actively hydrogen bonding with a silanol. To mimic the two-stage aldol condensation in our models, two different simulation environments were employed to depict each stage. Specifically, the first and second simulation environments contain 600 acetone and 600 4-nitrobenzaldehyde molecules, respectively, within the model pore on the crystalline silica surface with one or two alkylamine or alkylenamine functional groups. The MD simulations under the two different conditions were performed using the large-scale atomic/molecular massively parallel simulator (LAMMPS) package[49] with the DREIDING force field.[50] The total potential energy (E_{total}) is given as follows:

$$E_{total} = E_{vdW} + E_{Q} + E_{bond} + E_{angle} + E_{torsion} \quad (1)$$

where E_{vdW}, E_{Q}, E_{bond}, E_{angle}, and $E_{torsion}$ are the van der Waals, electrostatic, bond stretching, angle bending, and torsion components, respectively. The atomic charges were determined via Mulliken population analysis using density functional theory (DFT) with the B3LYP functional and 6-31G(d,p) basis set in the Jaguar package.[51] The detailed values for atomic charges are listed in the Supporting Information (Figures S1–S3). The Nose–Hoover thermostat and barostat were used to control the temperature and pressure in the isothermal–isobaric (NPT) ensemble (323 K and 1 atm) in the x and y directions for 5 ns. Charge-based coulombic interactions were calculated using the particle–particle particle–mesh (PPPM) solver.

RESULTS AND DISCUSSION

Characterization of Structural Properties of Alkylamine- and Alkylenamine-Functionalized Crystalline Silica Surfaces. Eight different crystalline silica surfaces were systematically modeled by introducing either an alkylamine or an alkylenamine, each of which had four different lengths of the alkyl chain from C1 (methyl) to C4 (butyl). The two types of MD simulations at 323 K and 1 atm corresponding to the experimental conditions[3−5,8,22] for the aldol condensation between acetone and 4-nitrobenzaldehyde were then performed. For the first stage, 600 acetone molecules were introduced in the systems, while for the second stage, 600 4-nitrobenzaldehyde molecules were introduced. Giving consideration to the aim of this study as a reference work to establish a well-designed simulation protocol that could be applied for more realistic, complicated models in future studies, we analyzed the MD simulation output from several points of view.

In the first analysis, we structurally characterized the time-evolved molecular behavior of the incorporated alkylamines and alkylenamines. Two different properties, namely, the flexibility of the alkyl linker and the distance between each acid–base pair, were investigated for all eight models. The time-evolved behavior and normalized distributions for the Si–N distances of the functional groups in the eight models are presented in Figure 3, quantifying the flexibility of each alkyl backbone. Here, Si and N represent the silicon atom of the grafted silane and the nitrogen atoms in either the alkylamine or alkylenamine (see Figure 1), respectively. Figure 3a confirms the alkyl linkers fluctuate throughout the entire simulation time. As expected, it is found that the Si–N distance increases with the number of carbon atoms in the alkyl linker of the functional group for both the alkylamine and alkylenamine. More importantly, it is also found that the time-dependent fluctuation of the Si–N distance is more significant as a function of the number of carbon atoms in the alkyl linker. This behavior is more pronounced for the alkylamine, exhibiting a stepwise change in the Si–N distance for C3 and C4 in Figure 3a,

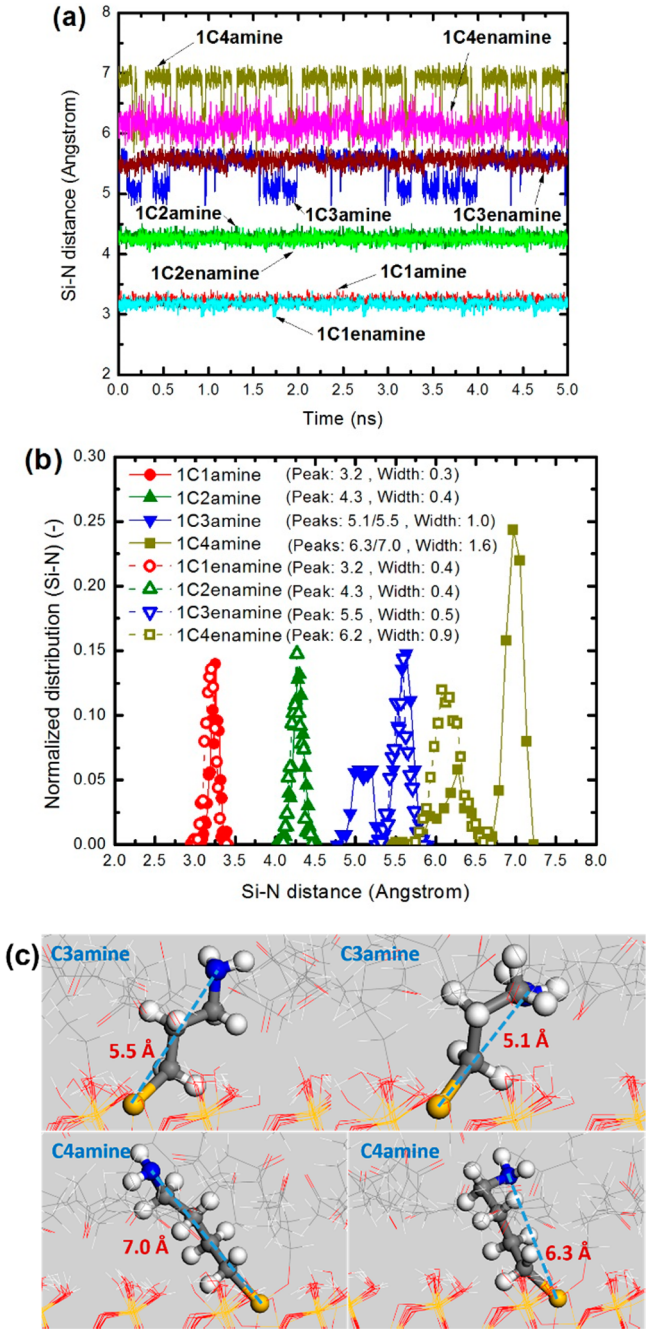

Figure 3. (a) Time-evolved Si–N distances and (b) their distributions for the alkylamine or alkylenamine functional groups of the eight different models. The peak position and width of each distribution in Å are listed in (b) for each of the eight models. Hereafter, 1Cn in each figure means one alkylamine or alkylenamine with n carbon atom(s) in the backbone. The extended and bent conformations for the C3 and C4 amines are illustrated in (c), with the Si–N distances in red.

compared to the alkylenamine functional group. For aminomethyl and aminoethyl groups, the Si–N distances did not significantly deviate from 3.2 and 4.3 Å for C1 and C2, respectively, during the simulations, which is due to the limited number of dihedral torsion angles that the C1 and C2 species can access. However, for the longer molecule, C3, the Si–N distance undergoes significant changes due to the degree of freedom associated with more accessible dihedral angles. This led to two peaks in Figure 3b: one (5.5 Å) for an extended

DOI: 10.1021/jacs.6b03309
J. Am. Chem. Soc. 2016, 138, 7664−7672

conformation and another (5.1 Å) for a bent conformation. Thus, the longest linker in our study, C4, has even larger fluctuations, as observed in Figure 3a,b. The peak positions for the Si−N distance are 7.0 and 6.3 Å for the extended and bent conformations, respectively. On the other hand, it is observed that the Si−N distances of alkylenamines generally show less fluctuation in comparison to those of alkylamines. Another point noted in Figure 3 is that the Si−N distance of the C3 enamine has a single peak at 5.5 Å from its extended conformation, whereas that of the C4 enamine has a single peak at 6.2 Å from its bent conformation. To understand this interesting behavior, we calculated the bonded and nonbonded interaction energies for the extended and bent conformations. From the potential energy calculations, the C3 enamine is more stable in the extended conformation by 16 kcal/mol than in the bent conformation, whereas the C4 enamine is more stable in the bent conformation by 16 kcal/mol than in the extended conformation. The relative stability between the two conformations is mainly due to the electrostatic interaction between the C=C group and SiO_2 fragment bridging the alkylenamine with the silica surface. Note that the two carbon atoms in the C=C group have charges of 0.33 (for the C atom bonded with the N atom) and −0.33, while the SiO_2 fragment has one Si atom with a charge of 1.1 and two O atoms with charges of −0.64 ∼ −0.57.

Another structural property, namely, the proximity of each acid−base pair, provides a clear understanding of the spatial accessibility for the cooperative interactions between the acid and base sites. The proximities of such acid−base pairs are illustrated by the pair correlation functions (PCFs) between $N_{amine}/N_{enamine}$ (nitrogen in amine/enamine) and $O_{silanol}$ (oxygen in silanol) shown in Figure 4, as well as Figures S5 and S6 in the Supporting Information. Note that the PCFs describe how the number density of target atoms varies as a function of distance from the reference atom. Specifically, for the C1 and C2 cases having less conformational diversity, the $N_{amine}-O_{silanol}$ pair correlation is sharply defined at specific distances, whereas for the cases of C3 and C4 with more degrees of freedom in their conformations, the $N_{amine}-O_{silanol}$ pair correlation is not well-defined. It is noted in Figure 4a,b that once the alkylenamine is formed from the alkylamine, the pair correlation between the N and O is more sharply defined because the conformational diversity of alkylenamines is less than that of the alkylamines.

In the viewpoint of the catalytic cooperativity, all these structural properties suggest that the C3 and C4 cases could provide more effective cooperative acid−base interactions than the C1 and C2 cases because the former cases would access a larger number of configurations of reactant molecules fitting suitably into the space generated between the acidic silanols and a basic amine. It should be stressed that these simulation results are consistent with experimental results from a series of acid−base mesoporous aminosilica catalysts with alkylamines ranging from C1 to C5, in which the catalytic activity in the aldol condensation increased up to C3, but no more improvement was found beyond C3.[3]

Characterization of the Hydrogen Bonding Properties between the Surfaces and Reactants. As discussed in the previous section, sustaining such a structurally suitable surface environment is a prerequisite for an alkylamine-functionalized silica material to cooperatively catalyze the aldol reaction. We now turn to the analysis of the molecular interactions between the surface and reactants during the aldol condensation. In each

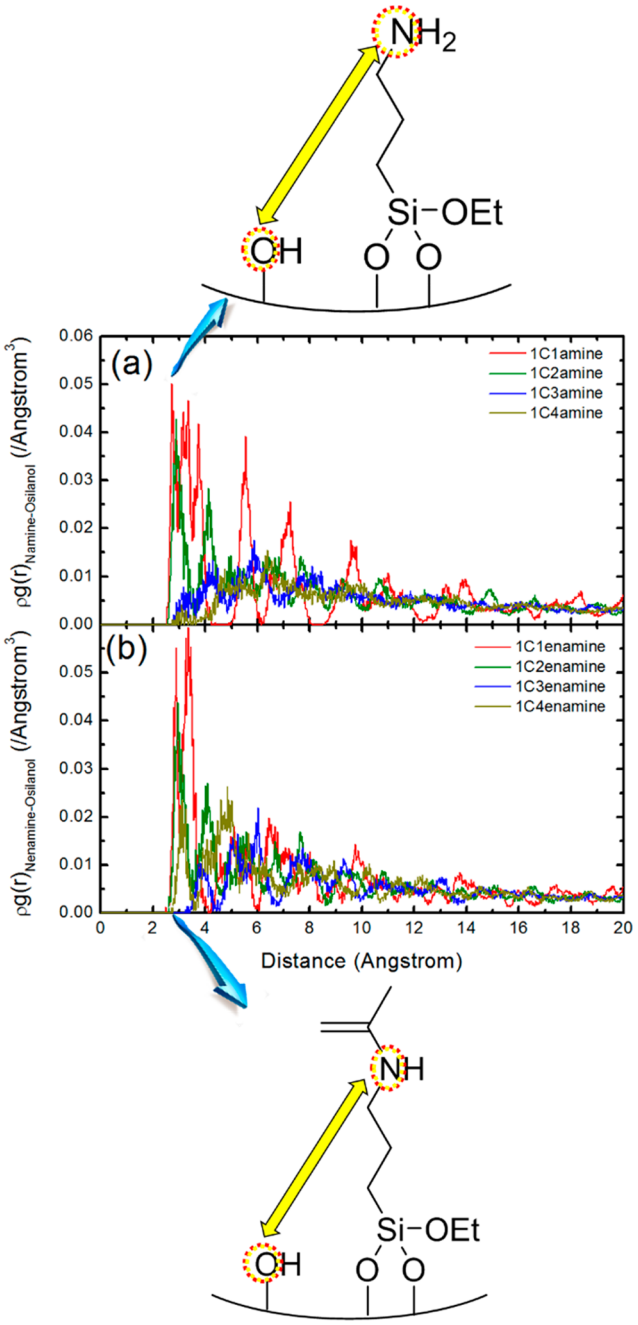

Figure 4. Pair correlation functions of $N_{amine}-O_{silanol}$ and $N_{enamine}-O_{silanol}$ pairs on a crystalline silica surface with one (a) alkylamine and (b) alkylenamine functional group, respectively. Here, N_{amine} (or $N_{enamine}$) and $O_{silanol}$ denote the nitrogen in a surface alkylamine (or alkylenamine) functional group and the oxygen in a surface silanol, respectively.

stage of the proposed two-stage aldol condensation mechanism,[23,31,32,46] a hydrogen bond between an acidic silanol (within reach of a basic alkylamine) and a reactant needs to be formed to prepare the reactant for nucleophilic attack by the basic amine. It is expected that the proton ($H_{silanol}$) of the silanol would attract (i) the oxygen of the carbonyl group of the acetone in the first stage and (ii) that of the 4-nitrobenzaldehyde in the second stage to form a hydrogen bond.[23,31,32,46] It is also expected from chemical intuition that a proton (H_{amine}) from the nitrogen in the alkylamine or alkylenamine might competitively form a hydrogen bond with

DOI: 10.1021/jacs.6b03309
J. Am. Chem. Soc. 2016, 138, 7664−7672

the reactant. The reactant forming a hydrogen bond with H_{amine} could be immobilized by the basic functional group such that the nucleophilic attack of the same basic functional group toward the reactant could be restrained. Therefore, the competitive behavior of $H_{silanol}$ and H_{amine} toward hydrogen bonding is a crucial factor affecting the cooperative catalytic activity.

To evaluate the hydrogen bonding interaction of reactants with the acidic or basic functional groups, the PCFs between $H_{silanol}$ and $O_{reactant}$ (oxygen of carbonyl in either acetone or 4-nirobenzaldehyde) as well as the PCFs between H_{amine} and $O_{reactant}$ were analyzed, as shown in Figures 5 and 6 (see Figures S7 and S8 in the Supporting Information for full information) as well as Figures S9 and S10 in the Supporting Information. One reasonable observation from Figures 5, 6, S7, and S8 is that the pair correlations of the silanol with the reactants are not affected by the length, number, or distribution of the basic functional groups. The reactants are predicted to consistently form hydrogen bonds with the silanols within a distance of 3 Å between $H_{silanol}$ and $O_{reactant}$, exhibiting the highest correlations at a distance of 2.1−2.2 Å. The difference in the intensity of the pair correlation between the alkylamine and alkylenamine cases is attributed to the nature of the simulated reactant, consistently exhibiting pair correlations for acetone higher than that for 4-nitrobenzaldehyde. This can be explained by the fact that each 4-nitrobenzaldehyde has oxygen atoms at both arms of the molecule, namely, the aldehyde and nitro groups, to form a hydrogen bond with a silanol. It is specifically validated from Figure S11 in the Supporting Information that a considerable number of the 4-nitrobenzaldyde molecules use the oxygen atoms in the nitro groups to form hydrogen bonds with the silanols. Compared with the clear pair correlations of the silanols with the reactants, the pair correlations between H_{amine} and $O_{reactant}$ in Figures S9 and S10 of the Supporting Information are not clear enough to be unambiguously interpreted.

For clearer understanding of the competitive hydrogen bonding interactions, we converted the PCF profiles to more understandable profiles, namely, the accumulated number (AN) of $O_{reactant}$ radially distributed around either $H_{silanol}$ or H_{amine}, as shown in Figures 7 and 8 (see Figures S12 and S13 in the Supporting Information for full information) as well as Figures S14 and S15 of the Supporting Information. Note that the AN describes how many target atoms are placed within a specific distance from a reference atom. In particular, based on the positions of the first solvation shells of $H_{silanol/amine}$ placed with a distance smaller than 3 Å (see Figures 5 and 6), the $O_{reactant}$ coordination numbers (CN) for each $H_{silanol/amine}$ to form a hydrogen bond were calculated as shown in the insets of these figures as well as in Tables S1 and S2 in the Supporting Information. Here, the CN describes the number of target

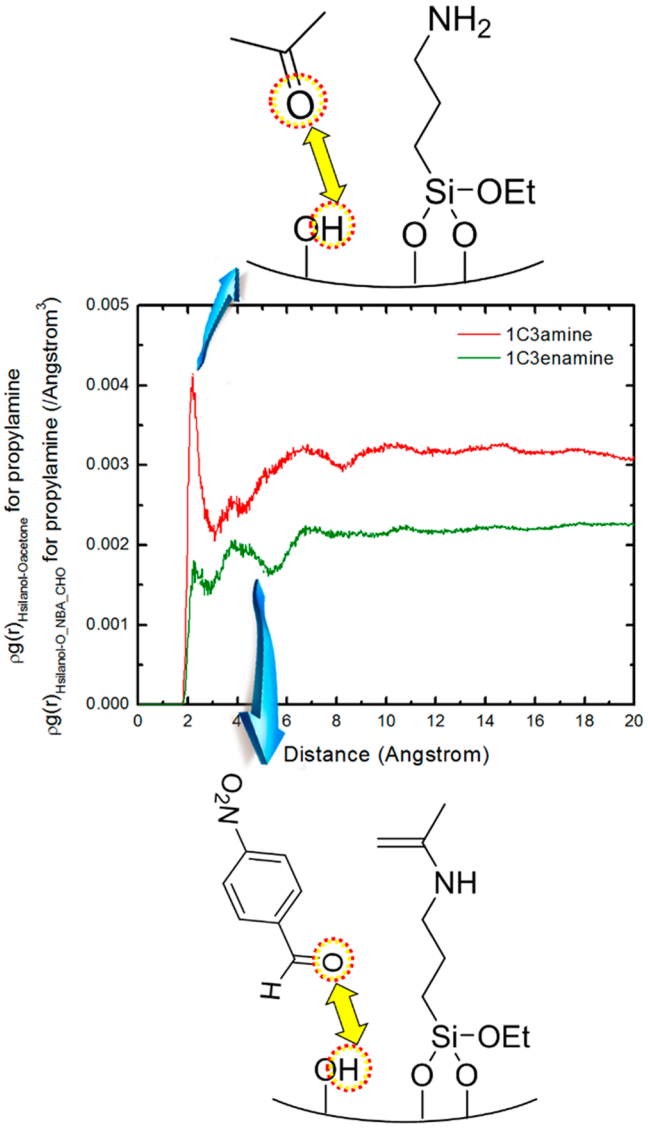

Figure 5. Pair correlation functions of $H_{silanol}$−$O_{acetone}$ and $H_{silanol}$−O_{NBA_CHO} pairs on a crystalline silica surface with one propylamine and propylenamine, respectively. Here, $H_{silanol}$ denotes the hydrogen in a surface silanol, and $O_{acetone}$ and O_{NBA_CHO} denote the oxygen of the carbonyl in acetone and 4-nitrobenzaldehyde, respectively. For clarity, only the C3 amine and C3 enamine are presented, whereas all other cases are presented in the Supporting Information.

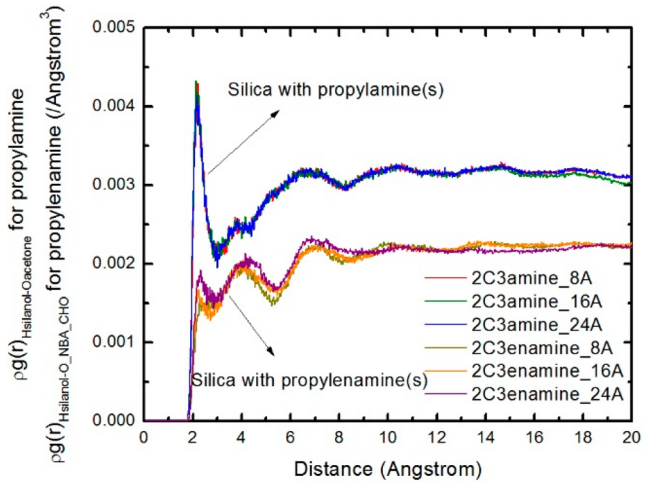

Figure 6. Pair correlation functions of $H_{silanol}$−$O_{acetone}$ and $H_{silanol}$−O_{NBA_CHO} pairs on a crystalline silica surface with two propylamines and propylenamines, respectively, at three different distances of 8, 16, and 24 Å between them. Here, $H_{silanol}$ denotes the hydrogen in a surface silanol, and $O_{acetone}$ and O_{NBA_CHO} denote the oxygen of the carbonyl in acetone and 4-nitrobenzaldehyde, respectively. Hereafter, 2C*n* amine_mA and 2C*n* enamine_mA in each figure mean two alkylamines and alkylenamines with *n* carbon atom(s) in the backbones, each of which is separated by the distance of *m* Å. As above, only the C3 amine and C3 enamine are presented, whereas all other cases are presented in the Supporting Information.

DOI: 10.1021/jacs.6b03309
J. Am. Chem. Soc. 2016, 138, 7664−7672

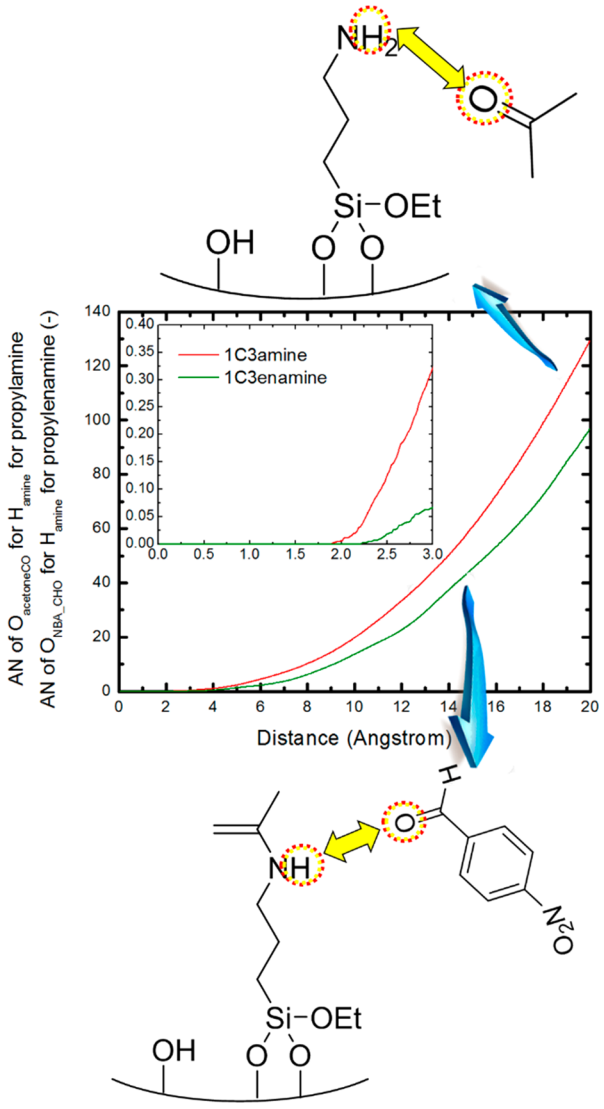

Figure 7. Accumulated number of $O_{acetone}$ and O_{NBA_CHO} radially distributed from each H_{amine} on the crystalline silica surface with one propylamine and propylenamine. Here, H_{amine} denotes the hydrogen forming a bond with nitrogen in an alkylamine or alkylenamine, and $O_{acetone}$ and O_{NBA_CHO} denote the oxygen of the carbonyl in acetone and 4-nitrobenzaldehyde, respectively. For clarity, only the C3 amine and C3 enamine are presented, whereas all other cases are presented in the Supporting Information. The figure is magnified in the inset to clearly describe the $O_{reactant}$ coordination numbers for each H_{amine}.

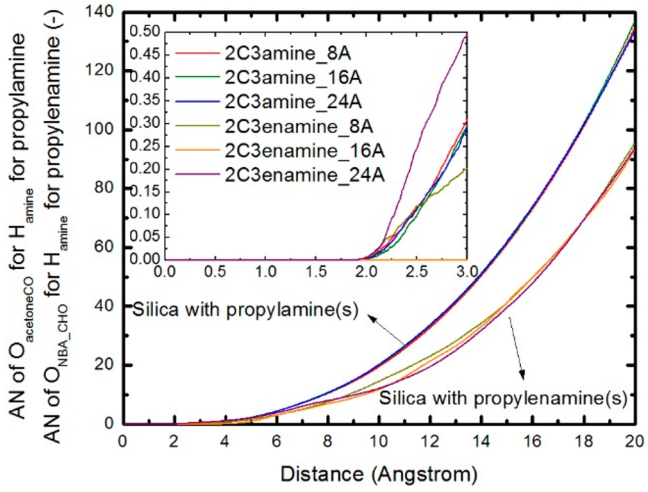

Figure 8. Accumulated number of $O_{acetone}$ and O_{NBA_CHO} radially distributed from each H_{amine} on the crystalline silica surface with two propylamines and propylenamines at three different distances of 8, 16, and 24 Å between them. Here, H_{amine} denotes the hydrogen forming a bond with nitrogen in an alkylamine or alkylenamine, and $O_{acetone}$ and O_{NBA_CHO} denotes the oxygen of the carbonyl in acetone and 4-nitrobenzaldehyde, respectively. For clarity, only the C3 amine and C3 enamine are presented, whereas all other cases are presented in the Supporting Information. The figure is magnified in the inset to clearly describe the $O_{reactant}$ coordination numbers for each H_{amine}.

atoms within a distance of 3 Å from the reference atom, which roughly corresponds to the positions of the first troughs in Figures 5 and 6. First, in the case of the hydrogen bonding between the silanol and the reactant, as expected from the PCF profiles, the CN consistently remained near 0.24 and 0.11−0.13 in the first and second stages of the two-stage aldol condensation mechanism,[23,31,32,46] respectively, regardless of the alkyl linker length, number, and distribution of the alkylamines/alkylenamines. It is worthwhile to note that the probability of forming a hydrogen bond between $H_{silanol/amine}$ and the aldehyde oxygen of 4-nitrobenzaldehyde in the second stage was half that of forming a hydrogen bond between $H_{silanol/amine}$ and acetone in the first stage. This is hypothesized to result from one or more of four factors: (1) the difference in size between the two reactant molecules; (2) the steric hindrance due to the enamine fragment; (3) the ability of three oxygen atoms at both arms of the 4-nitrobenzaldehyde, namely, the aldehyde and nitro group, to form a hydrogen bond; and (4) the increased electronegativity of the carbonyl oxygen of the acetone compared to that of the aldehyde oxygen of the 4-nitrobenzaldehyde. More surprising results are observed from the case of the hydrogen bonding between the alkylamine/alkylenamine and reactants. In the first stage, the alkylamine has a higher probability of forming a hydrogen bond with the acetone by 0.01−0.15 than the silanol. This is somewhat surprising because it is generally known that the OH−O hydrogen bond is substantially stronger than the NH−O hydrogen bond.[52] This observation might result from the difference in the available volume between the alkylamine and silanol for the approaching acetone. This suggests that the alkylamine would sterically hinder the neighboring silanol in activating the acetone to further catalyze the process. On the other hand, the ability of the alkylamine to form a hydrogen bond dramatically decreases by becoming the alkylenamine in the second stage, except for a few models with longer alkylenamines (either isolated or clustered cases), possibly due to the aforementioned factors. Such a drastic decrease in the ability of the basic functional group to form a hydrogen bond facilitates the activation of 4-nitrobenzaldehyde by the silanol.

Characterization of Reactive Pathways Catalyzed by Alkylamine Functional Groups. In each stage of the proposed two-stage aldol condensation mechanism,[23,31,32,46] the reactants stabilized by the silanol are catalyzed by the nucleophilic attack of the amine group at the first stage or the C−C double bond in the alkylenamine fragment in the second stage. The nucleophilic attack plays a critical role in catalyzing the aldol condensation, while the silanol-based catalytic activation is a process necessary to achieve enhanced catalytic activity in the reaction. To evaluate the catalytic activity, we

DOI: 10.1021/jacs.6b03309
J. Am. Chem. Soc. 2016, 138, 7664−7672

investigated the PCFs between N_{amine} and $C_{acetoneCO}$ and the PCFs between $C_{enamineCH_2}$ and C_{NBA_CHO}, as shown in Figures S16 and S17 of the Supporting Information, respectively. Figures 9 and 10 (see Figures S18 and S19 in the Supporting Information for full information) show the AN of $C_{acetoneCO}$ (C_{NBA_CHO}) radially distributed from each N_{amine} ($C_{enamineCH_2}$), converted from the PCF profiles. Each plot provides an insight into the probability of N_{amine} ($C_{enamineCH_2}$) approaching the carbon of the carbonyl in the acetone (4-nitrobenzaldehyde) for the nucleophilic attack. It is inferred from the figures that the expected catalytic activity is generally dependent on the length and flexibility of the alkyl linker. Thus, in the first stage, the C3 amines and C4 amines with flexible linkers are expected to have relatively high catalytic activity compared to the C1 amines and C2 amines. On the other hand, such a trend is not observed from the second stage where the flexibility of the alkyl linker is not significantly varied with its length.

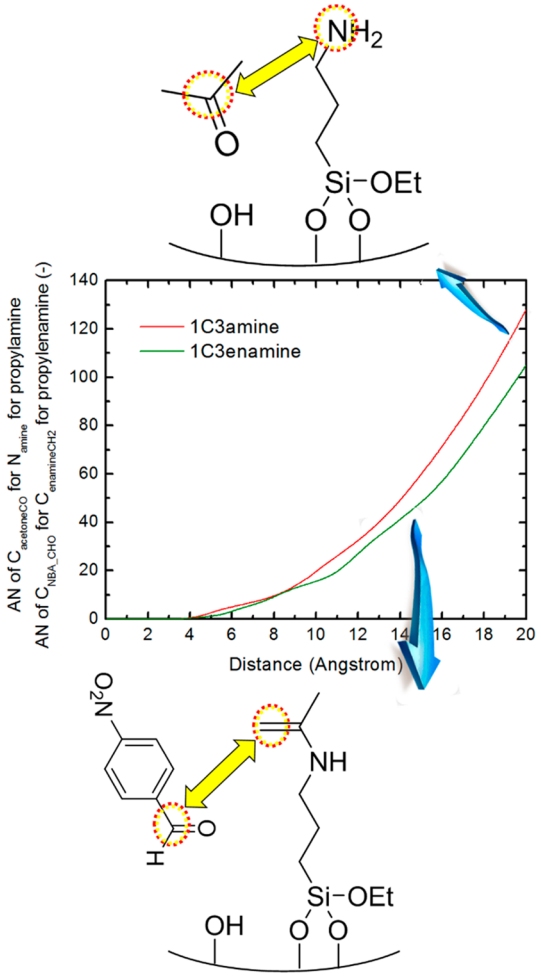

Figure 9. Accumulated number of $C_{acetoneCO}$ and C_{NBA_CHO} radially distributed from each N_{amine} and $C_{enamineCH_2}$, respectively, on a crystalline silica surface with one propylamine and propylenamine. Here, N_{amine} denotes the nitrogen in an alkylamine or alkylenamine, and $C_{acetoneCO}$ and C_{NBA_CHO} denote the carbon of carbonyl in acetone and 4-nitrobenzaldehyde, respectively. For clarity, only the C3 amine and C3 enamine are presented, whereas all other cases are presented in the Supporting Information.

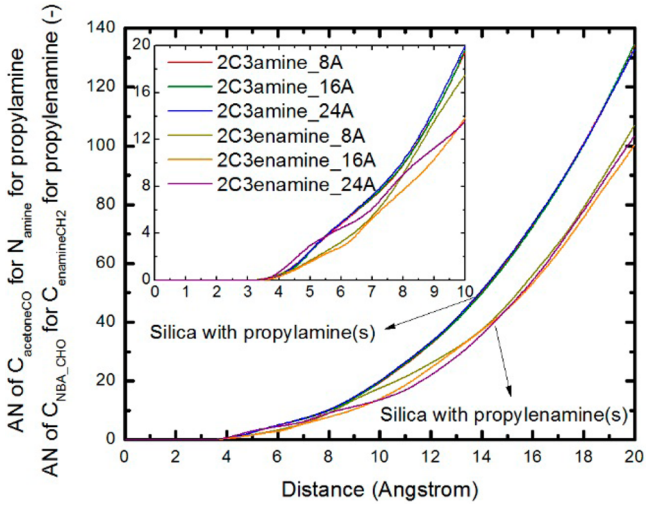

Figure 10. Accumulated number of $C_{acetoneCO}$ and C_{NBA_CHO} radially distributed from each N_{amine} and $C_{enamineCH_2}$, respectively, on a crystalline silica surface with two propylamines and propylenamines at three different distances of 8, 16, and 24 Å between them. Here, N_{amine} denotes the nitrogen in an alkylamine or alkylenamine, and $C_{acetoneCO}$ and C_{NBA_CHO} denote the carbon of the carbonyl in acetone and 4-nitrobenzaldehyde, respectively. For clarity, only the C3 amine and C3 enamine are presented, whereas all other cases are presented in the Supporting Information. The figure is magnified in the inset to clearly describe the AN within the two threshold distances, namely, 5 and 10 Å.

All the figures lead to one main conclusion: the effect of the alkyl length and spacing between the two alkylamines or alkylenamines on the catalytic activity would rely on the threshold distance within which the nucleophilic attack is assumed to occur. Note that all the reactant molecules within the threshold distance might be able to participate in the catalytic reaction, and the reactant molecules beyond the distance of 20 Å would not be relevant to the catalytic reaction. For example, if we assume that the nucleophilic attack can occur within 20 Å, the order of expected catalytic activity in the case of two alkylenamine functional groups would be 2C4 enamine_8A ≈ 2C3 enamine_8A > 2C2 enamine_8A > 2C1 enamine_8A at the threshold distance of 20 Å, while different orders would be expected at other distances. Table 1, numerically describing the AN at three different distances of 20, 10, and 5 Å, provides a clearer understanding of this conclusion. In other words, it is observed from Table 1 that the order of the expected catalytic activity would depend on the choice of the threshold distance. For example, in the case of the one alkylenamine, the order of the AN would be C3 > C1 > C2 > C4, C3 > C1 > C2 > C4, and C1 > C3 > C4 > C2 at the distance of 20, 10, and 5 Å, respectively, as shown in Table 1. Another interesting observation from Table 1 is the difference in the trend of the order of the expected catalytic activity between the alkylamine and alkylenamine cases. Specifically, in the alkylamine case, as the alkyl length of the alkylamine increases (regardless of the density and distribution of the functional groups), the expected catalytic activity is increased rapidly until C3 and then levels off from C3. However, such a trend is not observed from the cases for the alkylenamine. Considering the flexibility of the alkylamine/alkylenamine reported in Figure 3, the results in Table 1 suggest that the total number of reactants interacting with alkylamines/

DOI: 10.1021/jacs.6b03309
J. Am. Chem. Soc. 2016, 138, 7664−7672

Table 1. Accumulated Number of $C_{acetoneCO}$ and C_{NBA_CHO} Radially Distributed from Each N_{amine} and $C_{enamineCH_2}$, Respectively, within Three Different Threshold Distances of 20, 10, and 5 Å[a]

	AN ($C_{acetoneCO}$)					AN (C_{NBA_CHO})			
type	20 Å	10 Å	5 Å	onset (Å)	type	20 Å	10 Å	5 Å	onset (Å)
1C1 amine	117	15.4	1.77	3.19	1C1 enamine	94.4	14.4	1.81	3.29
1C2 amine	122	16.7	1.99	3.29	1C2 enamine	93.8	12.5	0.86	3.15
1C3 amine	128	19.7	2.53	3.19	1C3 enamine	105	15.6	1.15	3.15
1C4 amine	137	21.0	2.61	3.21	1C4 enamine	81.9	10.9	0.96	3.23
2C1 amine_8 Å	115	15.1	1.61	3.17	2C1 enamine_8 Å	91.6	12.3	2.01	3.31
2C1 amine_16 Å	114	15.4	1.67	3.31	2C1 enamine_16 Å	90.8	13.0	0.61	3.43
2C1 amine_24 Å	115	15.3	1.72	3.27	2C1 enamine_24 Å	93.5	12.3	2.49	3.21
2C2 amine_8 Å	118	15.6	1.80	3.17	2C2 enamine _8 Å	96.4	13.4	1.07	3.45
2C2 amine_16 Å	122	17.5	2.17	3.17	2C2 enamine_16 Å	90.0	11.2	1.23	3.29
2C2 amine_24 Å	119	17.1	2.19	3.17	2C2 enamine_24 Å	91.2	12.0	1.75	3.27
2C3 amine_8 Å	134	19.5	2.51	3.19	2C3 enamine _8 Å	107	17.5	1.71	3.11
2C3 amine_16 Å	135	19.7	2.46	3.23	2C3 enamine_16 Å	100	13.9	1.56	3.35
2C3 amine_24 Å	133	20.1	2.54	3.19	2C3 enamine_24 Å	103	13.6	2.96	3.25
2C4 amine_8 Å	139	20.4	2.48	3.21	2C4 enamine_8 Å	106	13.0	2.00	3.05
2C4 amine_16 Å	133	20.6	2.33	3.23	2C4 enamine_16 Å	106	18.2	1.91	3.39
2C4 amine_24 Å	142	21.8	2.50	3.21	2C4 enamine_24 Å	106	14.4	2.47	3.21

[a]Onset distance in Å is also listed for each model.

alkylenamines would increase with increasing linker flexibility, which shows the highest AN in the C3 and C4 amine cases. This observation rationalizes the work of Jones and co-workers reporting the trend in the cooperative catalytic activity of acid−base pairs on alkylamine-functionalized mesoporous silica surfaces with a series of alkyl linker lengths.[3] In contrast, the order of expected catalytic activity for the case of alkylenamine is hardly affected by the alkyl linker length because the flexibility is restricted by the incorporated enamine fragment. The electron-withdrawing nitro group in 4-nitrobenzaldehyde decreases the electron density at the aldehyde, increasing its electrophilicity.[7] Additionally, ketones are weaker electrophiles than aldehydes, so it is not surprising that activating the acetone is more difficult than activating the 4-nitrobenzaldehyde. Logically, it follows that the catalytic activity is unaffected by the length of the alkylenamine because the 4-nitrobenzaldehyde is a stronger electrophile than the acetone. As discussed, the aldol condensation mechanism is sequential: the acetone must undergo nucleophilic attack by the amine before the 4-nitrobenzaldehyde undergoes nucleophilic attack by the enamine.[3,4,7,23] If the hydrogen bonding between the acetone and the amine and the steric blocking of the silanols by the alkyl backbone both prevent the acetone from hydrogen bonding with the silanol, it makes sense that the first stage of the two-stage mechanism appears to limit the catalytic activity. From these results, it is likely that the rate-determining step of this aldol condensation is the nucleophilic attack of the acetone by the amine, as discussed in our previous experimental studies.[3,4]

It is important to note that our investigation has a few limitations that limit our ability to fully understand the observations of the cooperative aldol condensation despite the qualitative agreement of our simulation results with experimental observations. First, our simulation models are prepared based on crystalline silica surfaces with regularly positioned Si and O atoms such that the surface heterogeneity and pore curvature are not featured in our models. Second, unlike the quantum mechanical method, our simulation approach is not able to describe the chemical reaction to form chemical bonds during the reactions. Due to these aspects, our study has a significant limitation in producing a quantitative analysis of the cooperatively catalyzed aldol condensation. However, it should be emphasized that we have focused on the effect of the flexibility of the alkyl linker on the cooperative catalytic activity to isolate this important factor from the effects of other variables.

CONCLUSIONS

Alkylamine- or alkylenamine-grafted crystalline silica surfaces were studied via MD simulations to achieve a fundamental understanding of the cooperativity between amines and silanols, as well as probable reaction pathways in the aldol condensation between acetone and 4-nitrobenzaldehyde. A series of pair correlations between the acid−base functional groups and reactants were then analyzed while considering the proposed two-stage aldol condensation mechanism. It was found from this investigation that the cooperative catalytic activity of the acidic silanols and basic amines was mainly affected by two factors: (1) the competition between the silanol and the amine (or enamine) to form a hydrogen bond with a reactant and (2) the flexibility of the alkylamine. Our investigation on the competition concludes that the catalytic activation of the acetone by the silanol would be impeded by the basic functional group in the first stage of the proposed reaction mechanism while the 4-nitrobenzaldehyde activation by the silanol would be enhanced in the second stage because the hydrogen bonding between the amine and reactant is not possible. When combined with the reduced electrophilicity of the acetone and the increased probability of the acetone hydrogen bonding with the amine, it is likely that the rate-determining step of this aldol condensation is the nucleophilic activation of the acetone by the alkylamine. We further found that the activated (protonated) reactant would be subsequently catalyzed by the neighboring amine and enamine in the first and second stage, respectively, exhibiting the highest probability in the C3 and C4 amine functional group cases. In conclusion, the systematic simulation study on the aldol condensation using a simple bifunctional acid−base catalyst surface provides insights that

DOI: 10.1021/jacs.6b03309
J. Am. Chem. Soc. 2016, 138, 7664−7672

correlate the molecular interaction of the reactants and active sites with the catalytic reaction mechanism. This study sheds light on the potential of utilizing a molecular modeling approach to gain insight into complicated systems such as catalytic reactions on amine-functionalized mesoporous SBA-15 surfaces.

■ ASSOCIATED CONTENT

Supporting Information

The Supporting Information is available free of charge on the ACS Publications website at DOI: 10.1021/jacs.6b03309.

Tables S1 and S2 and Figures S1−S19 (PDF)

■ AUTHOR INFORMATION

Corresponding Authors

*cjones@chbe.gatech.edu

*seungsoon.jang@mse.gatech.edu

Notes

The authors declare no competing financial interest.

■ ACKNOWLEDGMENTS

We thank the U.S. Department of Energy, Office of Basic Energy Sciences, for funding this work through Catalysis Contract DEFG02-03ER15459. We also acknowledge that this research used resources of the Keeneland Computing Facility at the Georgia Institute of Technology, supported by the National Science Foundation under Contract OCI-0910735.

■ REFERENCES

(1) Kresge, C. T.; Leonowicz, M. E.; Roth, W. J.; Vartuli, J. C.; Beck, J. S. *Nature* **1992**, *359*, 710.

(2) Beck, J. S.; Vartuli, J. C.; Roth, W. J.; Leonowicz, M. E.; Kresge, C. T.; Schmitt, K. D.; Chu, C. T.-W.; Olson, D. H.; Sheppard, E. W.; McCullen, S. B.; Higgins, J. B.; Schlenker, J. L. *J. Am. Chem. Soc.* **1992**, *114*, 10834.

(3) Brunelli, N. A.; Didas, S. A.; Venkatasubbaiah, K.; Jones, C. W. *J. Am. Chem. Soc.* **2012**, *134*, 13950.

(4) Brunelli, N. A.; Jones, C. W. *J. Catal.* **2013**, *308*, 60.

(5) Brunelli, N. A.; Venkatasubbaiah, K.; Jones, C. W. *Chem. Mater.* **2012**, *24*, 2433.

(6) Lauwaert, J.; Moschetta, E. G.; Van Der Voort, P.; Thybaut, J. W.; Jones, C. W.; Marin, G. B. *J. Catal.* **2015**, *325*, 19.

(7) Collier, V. E.; Ellebracht, N. C.; Lindy, G. I.; Moschetta, E. G.; Jones, C. W. *ACS Catal.* **2016**, *6*, 460.

(8) Moschetta, E. G.; Sakwa-Novak, M. A.; Greenfield, J. L.; Jones, C. W. *Langmuir* **2015**, *31*, 2218.

(9) Maschmeyer, T.; Rey, F.; Sankar, G.; Thomas, J. M. *Nature* **1995**, *378*, 159.

(10) Jiao, F.; Frei, H. *Angew. Chem., Int. Ed.* **2009**, *48*, 1841.

(11) Takahashi, H.; Li, B.; Sasaki, T.; Miyazaki, C.; Kajino, T.; Inagaki, S. *Chem. Mater.* **2000**, *12*, 3301.

(12) Crudden, C. M.; Sateesh, M.; Lewis, R. *J. Am. Chem. Soc.* **2005**, *127*, 10045.

(13) Huh, S.; Chen, H.-T.; Wiench, J. W.; Pruski, M.; Lin, V. S.-Y. *Angew. Chem., Int. Ed.* **2005**, *44*, 1826.

(14) Kim, S.-W.; Son, S. U.; Lee, S. I.; Hyeon, T.; Chung, Y. K. *J. Am. Chem. Soc.* **2000**, *122*, 1550.

(15) Zornoza, B.; Téllez, C.; Coronas, J. *J. Membr. Sci.* **2011**, *368*, 100.

(16) Zelenak, V.; Halamova, D.; Gaberova, L.; Bloch, E.; Llewellyn, P. *Microporous Mesoporous Mater.* **2008**, *116*, 358.

(17) Newalkar, B. L.; Choudary, N. V.; Kumar, P.; Komarneni, S.; Bhat, T. S. G. *Chem. Mater.* **2002**, *14*, 304.

(18) Jang, K.-S.; Kim, H.-J.; Johnson, J. R.; Kim, W.-g.; Koros, W. J.; Jones, C. W.; Nair, S. *Chem. Mater.* **2011**, *23*, 3025.

(19) Bollini, P.; Didas, S. A.; Jones, C. W. *J. Mater. Chem.* **2011**, *21*, 15100.

(20) Slowing, I. I.; Trewyn, B. G.; Giri, S.; Lin, V. S.-Y. *Adv. Funct. Mater.* **2007**, *17*, 1225.

(21) Tang, F.; Li, L.; Chen, D. *Adv. Mater.* **2012**, *24*, 1504.

(22) Moschetta, E. G.; Brunelli, N. A.; Jones, C. W. *Appl. Catal., A* **2015**, *504*, 429.

(23) Lauwaert, J.; De Canck, E.; Esquivel, D.; Thybaut, J. W.; Van Der Voort, P.; Marin, G. B. *ChemCatChem* **2014**, *6*, 255.

(24) Didas, S. A.; Kulkarni, A. R.; Sholl, D. S.; Jones, C. W. *ChemSusChem* **2012**, *5*, 2058.

(25) Young, P. D.; Notestein, J. M. *ChemSusChem* **2011**, *4*, 1671.

(26) Holewinski, A.; Sakwa-Novak, M. A.; Jones, C. W. *J. Am. Chem. Soc.* **2015**, *137*, 11749.

(27) Moore, J. K.; Sakwa-Novak, M. A.; Chaikittisilp, W.; Mehta, A. K.; Conradi, M. S.; Jones, C. W.; Hayes, S. E. *Environ. Sci. Technol.* **2015**, *49*, 13684.

(28) Didas, S. A.; Sakwa-Novak, M. A.; Foo, G. S.; Sievers, C.; Jones, C. W. *J. Phys. Chem. Lett.* **2014**, *5*, 4194.

(29) Alkhabbaz, M. A.; Bollini, P.; Foo, G. S.; Sievers, C.; Jones, C. W. *J. Am. Chem. Soc.* **2014**, *136*, 13170.

(30) Sharma, K. K.; Buckley, R. P.; Asefa, T. *Langmuir* **2008**, *24*, 14306.

(31) Margelefsky, E. L.; Zeidan, R. K.; Davis, M. E. *Chem. Soc. Rev.* **2008**, *37*, 1118.

(32) Kandel, K.; Althaus, S. M.; Peeraphatdit, C.; Kobayashi, T.; Trewyn, B. G.; Pruski, M.; Slowing, I. I. *ACS Catal.* **2013**, *3*, 265.

(33) Bass, J. D.; Solovyov, A.; Pascall, A. J.; Katz, A. *J. Am. Chem. Soc.* **2006**, *128*, 3737.

(34) Zeidan, R. K.; Hwang, S.-J.; Davis, M. E. *Angew. Chem., Int. Ed.* **2006**, *45*, 6332.

(35) Zeidan, R. K.; Davis, M. E. *J. Catal.* **2007**, *247*, 379.

(36) Diaz, U.; Brunel, D.; Corma, A. *Chem. Soc. Rev.* **2013**, *42*, 4083.

(37) Hruby, S. L.; Shanks, B. H. *J. Catal.* **2009**, *263*, 181.

(38) Gianotti, E.; Diaz, U.; Velty, A.; Corma, A. *Catal. Sci. Technol.* **2013**, *3*, 2677.

(39) Shylesh, S.; Wagener, A.; Seifert, A.; Ernst, S.; Thiel, W. R. *ChemCatChem* **2010**, *2*, 1231.

(40) Shylesh, S.; Thiel, W. R. *ChemCatChem* **2011**, *3*, 278.

(41) Hanna, D.; Shylesh, S.; Li, Y.-P.; Krishna, S.; Head-Gordon, M.; Bell, A. T. *ACS Catal.* **2014**, *4*, 2908.

(42) Shylesh, S.; Hanna, D.; Gomes, J.; Krishna, S.; Canlas, C. G.; Head-Gordon, M.; Bell, A. T. *ChemCatChem* **2014**, *6*, 1283.

(43) Shylesh, S.; Hanna, D.; Gomes, J.; Canlas, C. G.; Head-Gordon, M.; Bell, A. T. *ChemSusChem* **2015**, *8*, 466.

(44) Sankaranarayanapillai, S.; Sreekumar, S.; Gomes, J.; Grippo, A.; Arab, G. E.; Head-Gordon, M.; Toste, F. D.; Bell, A. T. *Angew. Chem., Int. Ed.* **2015**, *54*, 4673.

(45) Vansant, E. F.; Van Der Voort, P.; Vrancken, K. C. *Characterization and Chemical Modification of the Silica Surface*; Elsevier: Amsterdam, The Netherlands, 1995; Vol. *93*.

(46) Sakthivel, K.; Notz, W.; Bui, T.; Barbas, C. F., III *J. Am. Chem. Soc.* **2001**, *123*, 5260.

(47) Ritter, H.; Nieminen, M.; Karppinen, M.; Brühwiler, D. *Microporous Mesoporous Mater.* **2009**, *121*, 79.

(48) Brühwiler, D. *Nanoscale* **2010**, *2*, 887.

(49) Plimpton, S. *J. Comput. Phys.* **1995**, *117*, 1.

(50) Mayo, S. L.; Olafson, B. D.; Goddard, W. A. *J. Phys. Chem.* **1990**, *94*, 8897.

(51) *Jaguar*, version 7.6; Schrodinger, LLC: New York, 2009.

(52) Rudner, M. S.; Jeremic, S.; Petterson, K. A.; Kent, D. R., IV; Brown, K. A.; Drake, M. D.; Goddard, W. A., III; Roberts, J. D. *J. Phys. Chem. A* **2005**, *109*, 9076.

DOI: 10.1021/jacs.6b03309
J. Am. Chem. Soc. 2016, 138, 7664−7672